Three-Dimensional Correction for Spillover and Recovery of Myocardial PET Images

Johan Nuyts, Alex Maes, Matthias Vrolix, Christiaan Schiepers, Heinrich Schelbert, William Kuhle, Guy Bormans, Gert Poppe, Denis Buxton, Paul Suetens, Hilaire De Geest and Luc Mortelmans

Departments of Nuclear Medicine and Cardiology, and ESAT-Machine Intelligence and Imaging, K.U. Leuven, Belgium; and Department of Molecular and Medical Pharmacology, UCLA School of Medicine, Los Angeles, California

PET permits the quantification of myocardial blood flow, but is hampered by the limited spatial resolution of the PET images. **Methods:** We evaluated two methods for the correction of resolution effects in PET perfusion $^{13}NH_3$-ammonia images. In one model, the spillover and recovery coefficients are estimated in the kinetic modeling analysis. The new, second model uses an explicit delineation of the left ventricular wall and a convolution model for the system point spread function to compute the regional values of the spillover and recovery coefficients. **Results:** The new method is validated with phantom measurements. The two methods are evaluated on animal experiments using $^{13}NH_3$-ammonia. Both two- and three-compartment models were used to compute absolute flow values. Excellent linear correlations with microsphere data were obtained. The slope of the regression line was lower for corrections based on kinetic modeling as compared to convolution-based correction. In animal experiments, recovery coefficients of 59% for the myocardial wall and 86% for the blood pool were obtained. Spillover from the blood pool into the myocardial wall was 14%. **Conclusion:** The new correction method strongly suppresses spillover and recovery effects due to limited resolution.

Key Words: PET; recovery correction; myocardial perfusion

J Nucl Med 1996; 37:767–774

The spatial resolution of PET images is limited by several factors, such as detector size, positron range, scatter, filtering and motion of the organ being studied. The blurring effect of the resulting point spread function has been carefully studied by several authors (*1–7*). In the imaginary ideal image, the value at every voxel (element of a three-dimensional image) equals the activity concentration at the corresponding position in the object. In the real, blurred image, this activity is distributed over a larger region. This blurring is usually described using two parameters: the recovery coefficient and the spillover coefficient. In order to accurately assess perfusion in the left ventricular (LV) wall using kinetic modeling analysis, correction for the resolution effect is required.

Two types of correction techniques have been proposed. In the first type, the resolution effects are included in the tracer kinetic model as extra parameters, to be determined in the fitting procedure (*7–11*). In the second type, the correction is applied prior to the kinetic model analysis (*4,12–15*). Obviously, the methods of the second type need information on the size and shape of the organs under study and on the resolution of the camera. This information cannot be derived from the emission image alone, because of its limited resolution. This implies that information from other measurements or a priori knowledge has to be used (*12–16*).

In this paper, we present a new method that uses both types of correction techniques. The spillover from the right ventricular (RV) blood pool is introduced as an extra parameter in the kinetic model analysis. For the correction of recovery and spillover from the LV blood pool, we propose a three-dimensional extension of the method of Bol et al. (*15*). The method is applied here to determine myocardial perfusion using dynamic PET studies with $^{13}NH_3$. Obviously, the same method can be applied to heart studies with other tracers. We will refer to this new method as the CC or convolution-based correction method.

The CC method is compared to an existing one, in which an extra parameter, combining the effects of spillover from the blood pool into the wall and of the blood volume in the myocardial tissue, is included in the tracer kinetic modeling (*7,10*). This method will be called the KC or kinetic modeling-based correction method.

Comparison of these methods is useful given that they have different strengths and limitations. The CC method corrects not only the counts of the myocardial wall, but also the input function. On the other hand, it ignores variations in wall thickness and requires careful calibration. The KC method does not require a model for the PSF and wall motion effects. This is important, since such a PSF model may be difficult to derive, particularly when iterative reconstruction techniques are applied (*17*). Its limitations are that it tends to overestimate the recovery coefficient, and that shifting the regions towards the endocardium results in an increase of the variance on the estimated flow values.

The results of multiple measurements will be denoted by mean ± 1 s.d. The cutoff frequency of filters is specified relative to the sampling frequency which, for our tomograph (both at UCLA and K.U. Leuven, Model 931-8/12, CTI/Siemens), equals 1/3.1 mm. The properties of this system have been described earlier by Spinks et al. (*18*). In all cases, reconstructed images were decay-corrected.

MATERIALS AND METHODS

Correction Algorithm

A mathematical derivation of the new algorithm is presented in Appendix 1. The resulting equations are:

$$M_r = (M' - s_{ML}L'_0)/r_M \qquad \text{Eq. 1}$$

$$L = (L' - s_{LM}M_r)/r_L \qquad \text{Eq. 2}$$

where M' is the measured regional tracer concentration in the myocardial wall; L' is the measured regional LV blood-pool concentration; L'_0 is the mean value of L' over a small central region in the LV blood pool; M_r is the corrected regional tracer concentration in the wall, only affected by spillover from the RV blood pool; L is the corrected regional blood-pool concentration; s_{ML}, s_{LM} are spillover from LV blood pool into the myocardial wall and vice versa; and r_M, r_L are the recovery coefficients of the myocardial wall and the LV blood pool.

Received Feb. 10, 1995; revision accepted Oct. 18, 1995.

For correspondence or reprints contact: Johan Nuyts, MD, Department of Nuclear Medicine, University Hospital Gasthuisberg, Herestraat 49, 3000 Leuven, Belgium.

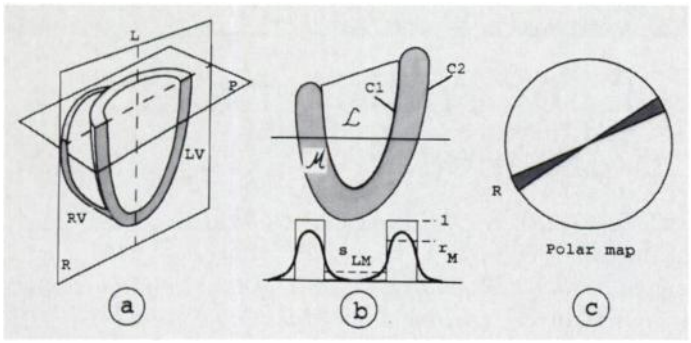

FIGURE 1. (A) A radial slice R. In all radial slices, the long axis of the LV coincides with the vertical center line. The slice in the figure cuts the RV. P is the basal plane. (B) C_1 and C_2 are the endocardial and epicardial contours. The horizontal profile through the myocardial wall $\mathcal{M}$ and the LV blood pool ($\mathcal{L}$) illustrates the procedure applied to compute the recovery and spillover coefficients (r_M and s_{LM}). (C) In dark, the contribution of a single radial slice to the polar map is represented.

Delineation of Myocardial Contours

To compute the regional spillover and recovery coefficients, outlines of the endocardium and the epicardium are needed. Since we have in-house software for automated delineation of myocardial emission tomograms (*19,20*), we have adjusted the input of the correction algorithm to the output of the delineation program. The delineation program uses radial slices. These are slices (usually 16) through the long axis of the LV wall, uniformly spread over 180° (Fig. 1A) (*20*). The delineation algorithm assumes that the tracer uptake in the LV wall is higher than in the surrounding tissue, as is the case in $^{13}NH_3$ and ^{18}FDG studies and SPECT perfusion studies. The program produces endo and epicardial contours for every slice and determines the position of the base by fitting a plane to the open end of the LV wall (Fig. 1A). This defines a complete three-dimensional delineation of the LV wall. LV thickness varies between 8 and 15 mm in humans (*21,22*) and 7 mm to 12 mm in dogs (echo measurements, described below). Since the overall resolution of the PET system is of the same order, wall thickness cannot be derived reliably from the PET image. Therefore, we currently impose a constant predefined wall thickness upon the contours (13 mm in human studies, 10 mm in dog studies).

Calculation of Left and Right Ventricular Blood-Pool Activity

The endocardial contour should adequately outline the LV blood pool. To reduce spillover from the myocardium, a new three-dimensional region is generated by shrinking the endocardial contour (factor 0.4) and shifting it upward until it touches the basal plane. This region will be referred to as the blood-pool region. The mean value of the blood-pool region is used as an estimate of the arterial tracer concentration of that particular time frame. The shrinking factor of 0.4 is an empirical compromise between minimization of the spillover (small region) and minimization of the noise on the mean value of the region (large region).

To correct for spillover from the RV blood pool into the myocardial wall, an approximate delineation of the right blood pool is made. First, all frames preceeding the LV blood pool peak value are added. RV blood-pool region is defined, consisting of all voxels less than 1.5 cm from the septum and exceeding an arbitrary threshold in the sum image (40% of the maximum, determined empirically). With this region, the RV blood pool time-activity curve is generated.

Calculation of Spillover and Recovery Coefficients

An idealized image of the LV wall is obtained by setting all voxels between the endocardial contour, the epicardial contour and the basal plane (region $\mathcal{M}$ in Fig. 1B) to unity and all other voxels to zero. If the PET system would be used to measure and reconstruct such a uniform distribution, a blurred image would be obtained because of the limited resolution and the beating of the heart. This blurring effect can be modeled by convolving the image with a blurring convolution kernel CK. Applying this to the idealized image results in a redistribution of the voxel values, as shown in Figure 1B. As a result, the value in the LV wall region $\mathcal{M}$ is decreased, while the value in the blood-pool region $\mathcal{L}$, originally zero, is slightly increased (Fig. 1B). By definition, the resulting value in $\mathcal{M}$ is the regional recovery coefficient r_M, and the value in $\mathcal{L}$ is the coefficient s_{LM} for spillover from $\mathcal{M}$ into $\mathcal{L}$. The blood-pool recovery r_L and the spillover s_{ML} from the blood pool into the wall are obtained in a similar way.

With these results, Equation 1 can be applied to compute the corrected wall values. A problem arises, however, when computing the product $s_{LM}M_r$ in Equation 2. Since the myocardial flow generally is not uniform, we have to determine which regional values M_r have contributed to the spillover in each of the blood pool voxels. To circumvent this problem, $s_{LM}M_r$ is directly computed by a procedure similar to the one described above. An idealized image is produced by retaining the inhomogeneous voxel values M_r in the region $\mathcal{M}$, while setting all other voxel values to zero. Convolution with CK produces the values $s_{LM}M_r$ in the blood-pool region $\mathcal{L}$.

The final corrected image is produced by applying Equations 1 and 2 on a voxel-by-voxel basis to the regions $\mathcal{M}$ and $\mathcal{L}$, respectively. The corrected input function is the mean value of L in the shrunken blood-pool region as a function of the frame time.

Derivation of Convolution Kernel

CK combines the blurring effects due to the limited camera resolution and the motion of the LV wall. Each of these two contributions can be represented by a PSF. We have carried out three experiments to measure these two PSFs separately.

The PSF of the tomograph was approximated by a sum of two Gaussians (*3,5,15*). In addition, we assumed that the tomograph PSF is isotropic. By smoothing in the direction perpendicular to the plane, the PSF can indeed be made nearly isotropic. This PSF was assessed with line source measurements, reconstructed and filtered in the same way as the cardiac studies. An additional experiment was performed to verify the assumption that CK is isotropic.

The wall motion PSF was derived from a gated study with eight frames per cycle. Radial slices were constructed and the myocardium was delineated for every frame. Based on these delineations, a Gaussian convolution kernel is derived, which has a blurring effect similar to the blurring induced by the wall motion. This kernel is the wall motion PSF.

The final kernel CK is a sum of two three-dimensional Gaussian kernels, obtained by convolving the wall motion PSF with the tomograph PSF.

Tracer Kinetic Model Analysis

From the delineated and corrected radial slices, two two-dimensional polar maps are computed (Fig. 1C). The count rate polar map contains the mean value of the central 7 mm between the endocardial and epicardial contours. Seven mm is an arbitrary compromise between reduction of spillover and noise suppression. The voxel sizes in this study ranged from 2.3 to 3.1 mm, so 3 to 4 voxels are averaged for a single polar map pixel. The volume polar map contains the myocardial volume in ml represented by each polar map pixel. Such a set of polar maps is computed for every time frame. Regions are automatically or manually defined, and for every region a time-activity curve is created.

In the animal experiments, the regions in the polar map were registered to the post-mortem tissue samples. The LV was cut along

the short-axis in three to five slices with equal thickness, and every slice was cut into eight sectors. The polar map was subdivided accordingly in three to five rings with eight overlapping regions of 4 to 6 ml per ring. The septum was used as a reference for alignment.

The input function was corrected for the presence of metabolites (*23*). Myocardial flow was estimated with a two-compartment (*16*) or three-compartment (*10*) modeling analysis (Appendix 2). In both models, the spillover from the right ventricular blood pool into the LV wall was included as an extra parameter. The two-compartment model was applied to the first 120 sec. The three-compartment model was applied to the entire dynamic set (10 min in the K.U. Leuven study, 4 min in the UCLA study).

Resolution Correction Based on Kinetic Modeling

Hutchins et al. (*7,10,11*) introduced an extra fitting parameter, the tissue blood volume, in the traditional three-compartment model, which estimates the combined effects of spillover from blood pool into myocardium and of the presence of arterial blood in the muscle. Excluding other sources of spillover, the recovery coefficient for the myocardial wall equals (1-tissue blood volume). In order to minimize spillover from structures outside the LV, the regions are drawn close to the endocardium (*7*). Therefore, we calculated an extra set of polar maps from the uncorrected radial slices, using the average voxel value between the mid-wall and the endocardium. The same approach was also applied to the two compartment model (Appendix 2).

Experiments

Convolution Kernel. A line source (plastic, internal diameter 1 mm, length 5 cm) was mounted in a 20-cm diameter acrylic cylinder, at 3.5 cm from the center of the cylinder, perpendicular to the reconstruction planes. The cylinder was filled with water. Three acquisitions were performed, each with a different position of the line source relative to the center of the camera's field of view: 0, 3 and 6 cm. In the reconstruction, Hanning filters with cutoff frequencies of 0.3 and 0.5 were used. The average radial profile through the center of the line spread function was determined. A sum of two Gaussians was fitted to this LSF profile.

In a second experiment, the same line source was mounted perpendicular to the axis of the same cylinder (parallel to the reconstruction planes). To improve the axial sampling, three acquisitions were performed with 2.25 mm interlacing in the z-axis. The images were reconstructed, using a Hanning filter with a cutoff of 0.3, and smoothed in the direction perpendicular to the planes with the convolution kernel (0.25, 0.5, 0.25). Axial and transaxial profiles through the line source were computed and a Gaussian curve was fitted to reduce noise artifacts. The FWHM of the Gaussians was calculated to compare the axial and transaxial resolution.

In a third experiment, the wall motion PSF was computed. Typical systolic and diastolic wall thicknesses were measured at 12 positions in each of 3 ultrasound images of dogs of similar weight. Four gated (8 frames/cycle) PET studies (3 baseline and 1 during adenosine stimulation) were performed. For each frame, a constant thickness was imposed onto the delineation. The thickness for the diastolic frame was set to the mean diastolic thickness obtained from the echo images. The thickness for the other frames was computed by requiring that the LV wall volume defined by the delineation was identical for all frames. As before, an artificial image was generated for each frame, assigning a value of 1 to voxels inside the delineated wall, and a value of 0 outside. Summing the 8 artificial images and dividing by 8 produced a blurred image. The convolution of a Gaussian kernel (simulating the blurring due to wall motion) and a rectangular profile (simulating the static wall profile) was fitted to profiles in the blurred image (using nonlinear least squares fitting). The estimated Gaussian is the wall motion PSF.

Phantom Measurements. In the first experiment, the corrected wall counts are compared to the counts in a phantom large enough to have a nearly perfect recovery. A cardiac phantom was mounted in an acrylic 20-cm diameter cylinder. The phantom simulates the LV wall (thickness 10 mm) surrounding a blood pool. The wall was filled with a homogeneous solution of ^{18}F. The blood pool and the cylinder were filled with water. The angle between the long axis of the cardiac phantom and the camera axis was 51° in the coronal view and 23° in the sagittal view. A cylindrical bottle (diameter 5.5 cm, height 9 cm) was filled with the same radioactive concentration as the wall and placed adjacent to the cylinder. An emission scan of 1 hr (total of 141 million counts) was performed. After an overnight decay of the radioactivity, a transmission scan was acquired for attenuation correction. The images were reconstructed (Hanning filter, cutoff frequency 0.3), and smoothed axially using a convolution mask (0.25, 0.5, 0.25). The corresponding radial slices were calculated and delineated. Polar maps were derived with and without recovery correction.

In a second experiment, the calculated spillover was compared to the true value, which was assessed with a dual-tracer study. The wall of the cardiac phantom was filled with ^{18}F, the blood pool with $^{13}NH_3$ and the cylinder with cold water. Initially the activity of the blood pool was about twice that in the wall with a total of 110 MBq. A dynamic study was performed and processed as in the previous experiment. The $^{13}NH_3$ values were corrected for ^{18}F contamination (less than 0.5% at end of bombardment). Nonlinear least squares fitting of the two decay exponentials was used to separate the contributions from $^{13}NH_3$ and ^{18}F in both the blood-pool region and in the polar map. The fitting results are used to calculate recovery and spillover coefficients before and after application of the CC method.

Animal Experiments. A first set of 12 PET experiments in 4 dogs was performed at UCLA to study flow under baseline and hyperemic conditions. The experimental setup has been previously described (*16*).

A second set of animal studies was conducted at K.U. Leuven, and evaluated flow under baseline and occlusion conditions. In contrast to the UCLA study, the apex was included in the data processing. Seven mongrel dogs of either sex, weighing 23 to 31 kg (mean 26.6 kg) were sedated intramuscularly with fluanisone (Hypnorm) 0.25 ml per kg body weight. After sedation, the dogs were anesthetized intravenously with Na-pentobarbital (Nembutal) 15 mg/kg, intubated and ventilated with air. Catheters were inserted in the left brachial vein (Nembutal infusion: 0.1 mg/kg/min), in the right brachial vein (heparin bolus: 5000 I.U. + infusion: 20 I.E./kg/hr) and in the left femoral artery (blood pressure monitoring and withdrawal of blood during injection of radioactive microspheres). A pigtail catheter was inserted in the LV through the left carotid artery, for injection of radioactive microspheres. In the right carotid artery a 9F sheath was placed for the insertion of a Stertzer catheter. A catheter was placed in the left jugular vein for blood withdrawal of $^{13}NH_3$ metabolites. Coronary angiography was performed in every dog. A balloon was inserted in the distal LAD or circumflex artery and the position verified. The dog was then transferred to the PET facility and positioned on its right side in the tomograph. ECG and blood pressure were monitored before, during and after balloon inflation. A 15-min transmission scan was performed to correct for photon attenuation. Then 560 MBq $^{13}NH_3$, distributed in 6 ml NaCl 0.9%, was infused at a rate of 10 ml/min, followed by a flush of 30 ml NaCl 0.9% at the same rate. Acquisition was started at the time of injection and 18 frames were acquired (1 × 20 sec, 10 × 10 sec, 2 × 20 sec, 2 × 40 sec, 3 × 120 sec). Blood samples for metabolite counting were taken at times: 1 min 20 sec, 2 min, 2 min 40 sec, 3 min 40 sec, 6 min and 10 min.

TABLE 1
Parameters of the Two Gaussian Distributions Modeling the Point Spread Function (Derived from Line Source Measurements)

Type	Ampli 1*	s.d. 1 [mm]†	Ampli 2 [10^{-4}]‡	s.d. 2 [mm]§	G2/G1¶ [%]
Han 0.3, 0 cm	1	5.00	3.46	27.6	5.8
Han 0.3, 3 cm	1	5.00	3.66	27.1	5.7
Han 0.3, 6 cm	1	5.06	3.76	27.1	5.7
Han 0.5, 0 cm	1	3.75	4.50	19.4	6.2
Han 0.5, 3 cm	1	3.79	4.76	19.2	6.2
Han 0.5, 6 cm	1	3.83	5.09	18.9	6.1

*The amplitude of the Gaussian distribution with the smallest s.d. was normalized to unity.

†s.d. of the first Gaussian distribution.

‡Amplitude of the second Gaussian distribution after normalization.

§s.d. of the second Gaussian distribution.

¶The ratio of the counts in the second Gaussian distribution divided by the counts in the first one. The counts are proportional to the integral of the Gaussian distribution over the three-dimensional space.

Seven baseline and four occlusion studies were performed in the seven dogs. Microspheres (^{95}Nb, ^{141}Ce and ^{103}Ru) were resuspended with a vortex shaker and injected as a bolus 60 sec after start of $^{13}NH_3$ injection. The calibration was carried out by withdrawal of arterial blood at a rate of 10 ml/min. Unmetabolized $^{13}NH_3$ in plasma was determined using the ion exchange method described by Bol et al. (*15*). All samples were recounted after decay of $^{13}NH_3$ (120 min) to measure the ^{18}F concentration.

Input Function. For the animal studies, the input function was determined before and after correction for recovery and spillover, and for different values of the shrinking factor defining the blood-pool region.

RESULTS

Convolution Kernel

The two Gaussian distributions, representing the tomograph PSF, are presented in Table 1. The amplitudes were normalized by assigning a value of 1 to the Gaussian distributions with the smallest s.d. Figure 2 shows the measured data and the fitted model for a line source measurement at 6 cm from the center. The second line source experiment resulted in a transaxial (in-plane) resolution of 13.2 mm FWHM and an axial resolution of 14.6 mm FWHM.

Wall thickness measured with ultrasound was 8.6 mm ± 1.3 at a diastole and 11.5 ± 1.3 at systole. The s.d. of the fitted Gaussian, describing the wall motion PSF, was 2.4 mm ± 0.1 mm. The profiles of the adenosine and rest studies were not different.

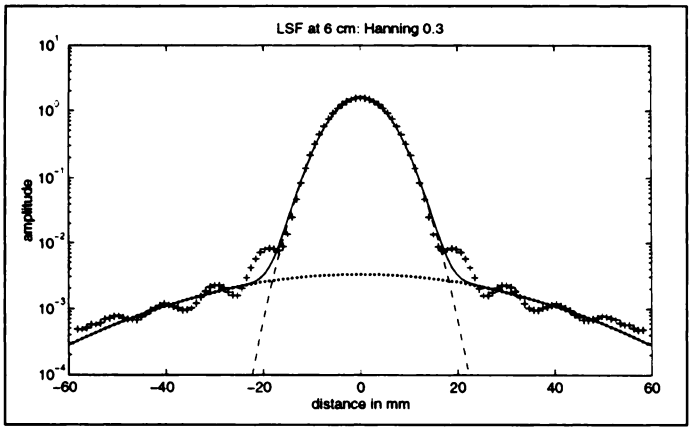

FIGURE 2. The measured line spread function (+), together with the two fitted Gaussian distributions (· · · and – –) and their sum (solid line), for a Hanning window with cutoff frequency at 0.3 and at 6 cm from the center.

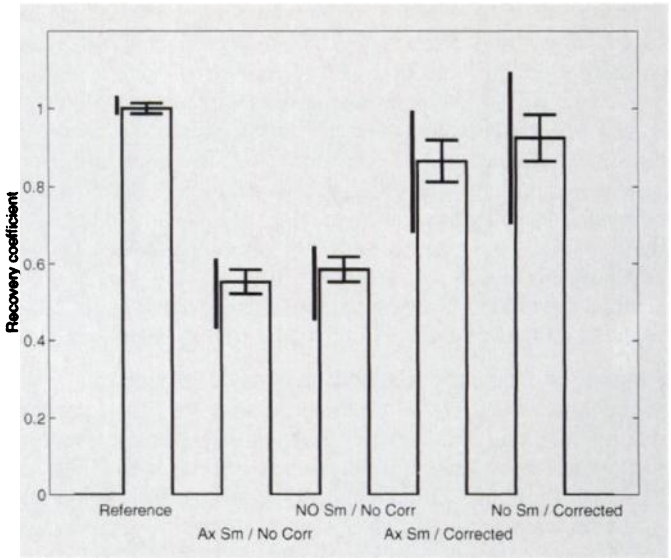

FIGURE 3. Recovery coefficients calculated from the first cardiac phantom measurement. The bars represent the mean values, the flags show the s.d. and the thick lines show the range. From left to right: the reference (perfect recovery assumed); axial smoothing, no correction (Ax Sm/No Corr); no axial smoothing, no correction (No Sm/No Corr); axial smoothing, correction CC (Ax Sm/Corrected); no axial smoothing, correction CC (No Sm/Corrected).

Phantom Measurements

Figure 3 shows the recovery coefficients, together with mean recovery value in the polar map for each of the four sets of radial slices (with and without smoothing, with and without correction), obtained from the first experiment. Axial smoothing decreases the recovery coefficient. The correction increases the recovery coefficient, but the corrected values are still slightly lower than the reference value. After correction (and axial smoothing) the mean recovery coefficient of the wall is 0.87 ± 0.06, with values ranging from 0.68 to 0.99.

Table 2 presents the results of the dual-tracer experiment. The recovery and spillover coefficients were computed using the recovery coefficient of the corrected wall from the first experiment and the fitted exponentials.

Animal Experiments

Linear regression was applied to compare the microsphere flow and the PET flow for every individual region and for mean flow values. In occlusion studies, a mean flow was computed for the occlusion territory, and a second one for the normal zone. In the baseline and hyperemic studies, the mean of all regions was computed. Flows were calculated applying the two- or three-compartment model, with or without correction for metabolites, and with one of the two presented corrections for spillover and recovery (CC or KC). Figure 4 shows the plots for the individual regions and the mean values for the two-

TABLE 2
Recovery and Spillover Coefficients Derived from Cardiac Phantom Measurements

	No correction	Corrected with CC method
Recovery wall	0.58	0.87
Recovery blood pool	0.92	1.00
Spillover wall to blood pool	0.044	0.010
Spillover blood pool to wall	0.096	0.023

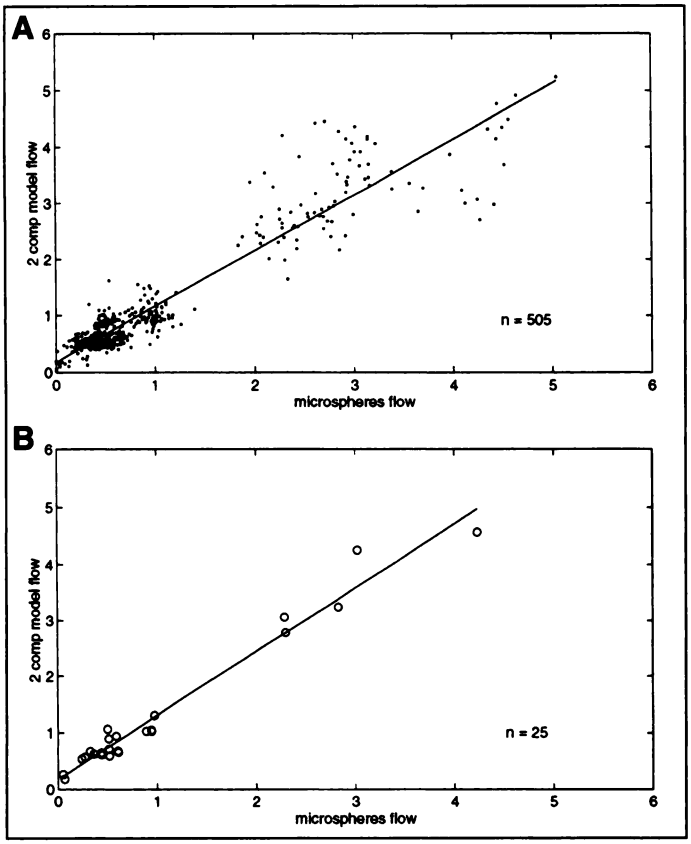

FIGURE 4. Flow values in individual regions (A) and the corresponding mean values (B) obtained by applying a two-compartment model with the convolution-based correction (CC) and correction for metabolites. The flow is expressed in ml/(g min).

TABLE 4
Spillover and Recovery Coefficients Computed by the Convolution Method in Animal Studies

	Mean	s.d.	Range
Recovery LV wall	0.59	0.046	0.35–0.63
Recovery blood pool	0.86	0.051	0.75–0.92
Spillover wall to blood pool	0.038	0.015	0.014–0.066
Spillover blood pool to wall	0.14	0.016	0.09–0.20

compartment model (method CC). The plots for the other combination of methods are very similar. In Table 3 the results of the regression analysis are presented. All correlations were significant ($p < 0.001$, t-test). The 95% confidence intervals are small, in particular for the individual regions, so most of the differences in slope are significant. For the individual regions, the slope obtained with the CC method was in all cases significantly higher than that with the KC method. Also, metabolites correction yielded a significantly higher slope. The spillover and recovery values are tabulated (Table 4). The calculated recovery values are uniform over the myocardium, except for a strong decrease near the base. The recovery coefficient near the apex is on the average 3% higher than in the rest of the wall.

The variance increases with increasing microspheres flow (Fig. 4). However, the relative error, defined as the s.d. of the estimated flows divided by the mean microspheres flow, did not correlate with the flow and amounts to approximately 20% for all methods.

In all cases there was a moderate negative correlation between microspheres flow and LS (L = left, S = spillover). (Depending on the model and the corrections used, LS represents only the fractional blood volume in the myocardium, or

TABLE 3
Results of Correction and Kinetic Modeling in Animal Studies

Model*	Corr†	Metab‡	Slope	cl95§	Intercept (ml/g · min)	r¶	s.e.e.** (ml/g · min)	LS
				Mean values				
2	KC	N	0.78	0.06	0.20	0.98	0.18	0.31 ± 0.05
2	KC	Y	0.82	0.06	0.22	0.98	0.19	0.31 ± 0.06
2	CC	N	0.92	0.07	0.19	0.98	0.21	0.09 ± 0.05
2	CC	Y	0.99	0.07	0.16	0.98	0.22	0.09 ± 0.05
3	KC	N	0.72	0.04	0.25	0.99	0.15	0.29 ± 0.08
3	KC	Y	0.79	0.05	0.26	0.99	0.15	0.29 ± 0.08
3	CC	N	0.79	0.05	0.33	0.99	0.15	0.08 ± 0.05
3	CC	Y	0.83	0.05	0.34	0.99	0.15	0.08 ± 0.05
				Individual values				
2	KC	N	0.77	0.02	0.23	0.94	0.29	0.31 ± 0.09
2	KC	Y	0.82	0.02	0.24	0.94	0.30	0.32 ± 0.10
2	CC	N	0.91	0.02	0.21	0.95	0.31	0.10 ± 0.09
2	CC	Y	0.99	0.02	0.18	0.95	0.34	0.10 ± 0.09
3	KC	N	0.71	0.02	0.28	0.96	0.22	0.29 ± 0.10
3	KC	Y	0.78	0.02	0.29	0.95	0.25	0.30 ± 0.11
3	CC	N	0.78	0.02	0.35	0.94	0.28	0.08 ± 0.08
3	CC	Y	0.82	0.02	0.36	0.94	0.31	0.08 ± 0.08

*Two- or three-compartment tracer kinetic model.
†KC or CC correction method.
‡Correction for metabolites in the blood: Yes or No.
§slope ± cl95 is the 95% confidence interval.
¶Regression coefficient obtained from linear regression.
**Standard error estimate (or s.d. about regression line).

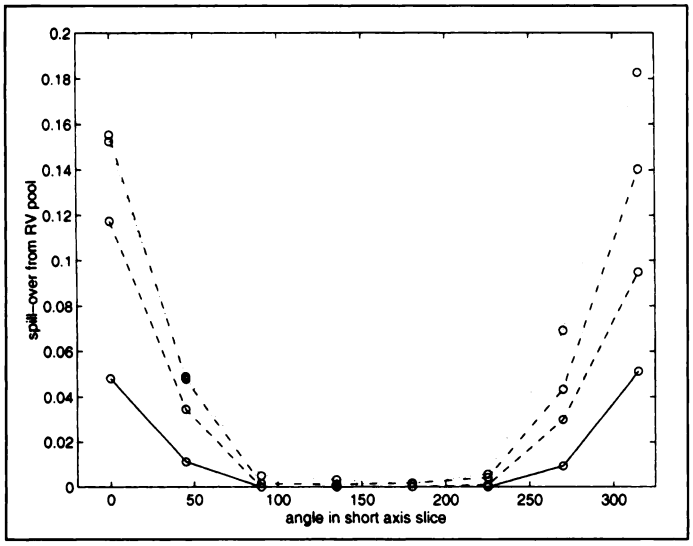

FIGURE 5. Mean coefficients of spillover from the RV blood pool into the wall, as a function of the angle in the polar map. The values were obtained by applying a two-compartment model with convolution-based correction (CC) and correction for metabolites. The center of the septum is at 0°. The mean for each region over all studies was calculated. Four rings of 8 regions are shown: —: ring 1, – –: ring 2, – · –: ring 3, · · ·: ring 4. Ring 1 is closest to the apex, ring 4 closest to the base.

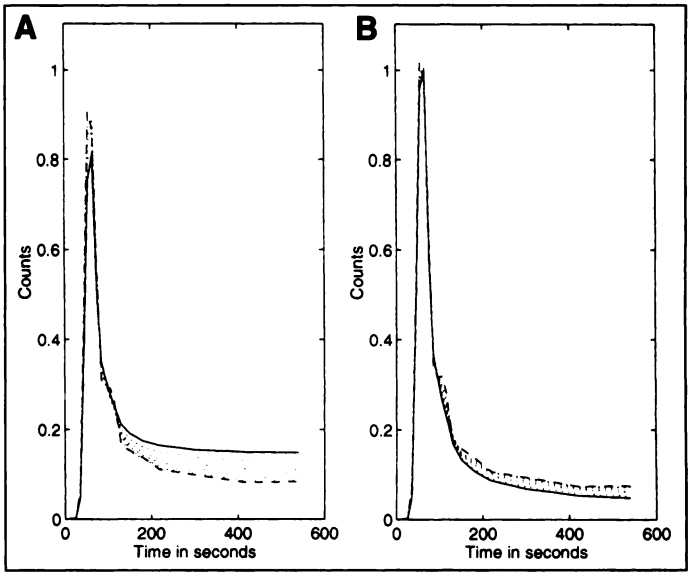

FIGURE 6. Typical blood-pool function (A) before and (B) after CC correction, for blood-pool regions with different sizes, relative to the region enclosed by the endocardial contour: – –: 0.2, —: 0.8. The dotted lines show the curves for the intermediate size (0.3–0.7).

the sum of the latter and the spillover from the LV blood pool.) The correlation was not significant in the two-compartment model ($r = -0.2 \cdots -0.4$, p = ns). It was significant in the three-compartment model using KC ($r = -0.61$, $p < 0.001$) and using CC ($r = -0.4$, $p < 0.05$). Correction for metabolites did not affect this correlation.

Figure 5 shows the values of the RV spillover obtained using the two-compartment model, the CC-method and correction for metabolites. The figure shows the mean values over all studies, as a function of the angle in the polar map. An angle of 0° corresponds to the center of the septum, 180° to the center of the lateral wall.

Input Function

Figure 6 shows the results of all the manipulations. Before correction, the larger blood-pool regions suffer more from spillover from the activity in the wall, resulting in higher activities in the later frames. The larger regions also have a lower recovery value and, consequently, a lower peak value in the first frames. After correction the influence of the region size is smaller. Note that even for the smallest regions, the recovery coefficient was only 0.9.

DISCUSSION

Assessment of Myocardial Wall Thickness

Bol et al. (*15*) have presented a correction method for finite resolution effects using manually defined heart regions and Monte Carlo simulation. Our CC method is a three-dimensional extension of their method. The use of a convolution kernel is equivalent to the Monte Carlo approach. An important difference, however, is the definition of the contours. Because the myocardial wall thickness is of the same order as the spatial resolution of the PET system, it cannot be estimated reliably from the PET images. We solved that problem by assuming a constant wall thickness (*15*) by relying on the manual skills of the operator. The image of a stationary wall is less blurred. As a result, it has a better recovery, but will appear thinner in the image, so manual delineation is likely to produce an overcorrection. On the other hand, a thinner wall has a lower recovery coefficient, which will be overestimated when a constant thickness is assumed. Currently, it is unclear which strategy would be preferable. The only correct, although elaborate, approach is the use of accurate anatomical information, such as gated MRI images.

Comparison of the Methods

Estimating the spillover and recovery coefficients with kinetic modeling techniques is difficult because insufficient information is available. The sum of the recovery coefficient and the coefficients of spillover from surrounding regions equals unity. Consequently, the recovery coefficient can be computed if all spillover coefficients are known, not only from the LV blood pool, but also from zones outside the LV wall. Except for the RV blood pool, however, these zones do not provide a useful time-activity curve, which is required to estimate the corresponding spillover coefficient. Shifting the regions towards the endocardium (*7*) reduces but does not eliminate the influence from those zones. This leads to an overestimation of the recovery and an underestimation of the flow, as shown in Table 3. In this study, assuming a constant thickness of 1 cm and applying the CC method resulted in a superior estimate of the recovery coefficients and, therefore, a better slope in the regression with microsphere flow values (Table 3).

The performance of the two correction methods is essentially equivalent, since the random variations, expressed as the standard error on the estimate, are similar. Consequently, the CC method is preferable in complex, multi-parameter systems, where the number of parameters to be estimated is large and should not be extended with extra recovery or spillover coefficients. On the other hand, in cases where iterative reconstruction techniques are used, the KC method may be superior. Liow et al. (*17*) showed that the resolution in an image produced by maximum likelihood expectation maximization in combination with a stopping rule is not uniform, but depends on the local image characteristics. Moreover, the local convergence depends also on global image content (*24*). As a result, it is not possible to derive a unique PSF for such images, and the CC method and similar approaches cannot be applied. Maximum likelihood-expectation maximization yields a better compromise between

resolution and noise and, as a result, the KC method will produce better slopes.

Absolute Flow Values

For all methods, excellent correlations were obtained. The two-compartment model produces lower intercept values, the three-compartment model produces slightly better correlations and lower s.e.e. values. The slope of the two-compartment model, combined with the CC method is equal to unity. For the three-compartment model, a lower slope is found. Since, however, the phantom measurements show that the CC method slightly undercorrects the resolution effects, it is probably fair to state that in this study, the two-compartment model tends to overestimate the flow while the three-compartment model tends to underestimate it.

In all our linear regressions between PET measurements and microspheres data, a positive intercept was obtained (Fig. 4, Table 3). Similar findings have been reported by other groups (*11,15,16*). This may be due to an artifactual increase in reconstructed count rate because of Compton scatter. Alternatively, diffusible tracers in the low flow range might always yield higher blood flow values when compared to the microsphere technique, due to an intrinsic difference between diffusible and corpuscular tracers. Hence, a distinction may have to be made between nutrient and capillary blood flow.

Application of metabolites correction improves the slope of the regression lines, but does not affect the regression coefficients or s.d.s about the regression line (Table 3). Similar findings were reported in (*15*).

Right Ventricular Blood Pool

Bol et al. (*15*) found a weaker correlation between microspheres and calculated flow for septal regions. This finding was attributed to spillover from the RV blood pool. Figure 5 shows that spillover from the RV is indeed present and that it can be identified in the septal regions by kinetic modeling analysis.

Limitations of the Convolution Method

One of the assumptions of the CC method is that the activity outside the heart is low, compared to the activity in the myocardial wall or the blood pool. This assumption is met in ^{18}FDG studies, but not always in the $^{13}NH_3$ studies. In some patients, the lung uptake is not negligible, so the lateral wall could be affected by spillover from the activity in the left lung. In some studies, the liver uptake is so high that the spillover may actually dominate the regional LV wall concentration.

The phantom measurements (Fig. 3, Table 2) show that the CC method strongly reduces the resolution effects. Complete correction, however, is not obtained due to the linear interpolation in creating the radial slices. Linear interpolation is equivalent to a convolution with a smoothing, triangular kernel followed by sampling. This effect has been carefully studied for short-axis slices by Kuhle et al. (*6*). They found that the loss in recovery depends on the angle of reorientation and typically amounts to 15% for a reorientation angle of 45°. This effect is ignored in the current implementation. Possible solutions are decreasing the voxel size or including the average interpolation effect in the system PSF.

CONCLUSION

We have compared two methods for the correction of resolution artifacts: one based on an explicit delineation of the myocardial wall and a convolution model for the spatial resolution, the other one estimating the blurring effects in the tracer kinetic modeling step. The first method was validated using phantom measurements. Both correction methods were combined with the two- and three-compartment kinetic models to estimate the absolute flow values in canine studies. Linear regression with microspheres flow resulted in excellent correlation for both methods, a better slope for the first method and no significant difference in random errors. Consequently, the kinetic modeling approach can be used in applications where no unique point spread function is available (such as in maximum likelihood-expectation maximization constrained by a stopping criterion). In contrast, the convolution method will be useful in cases where the resolution effects cannot be included as model parameters.

APPENDIX 1

The relation between the real tracer concentrations and the estimated values can be written as follows:

$$M' = r_M M + s_{ML} L + s_{MR} R + s_{ME} E \qquad \text{Eq. 3}$$

$$L' = r_L L + s_{LM} M \qquad \text{Eq. 4}$$

$$R' = r_R R + s_{RM} M \qquad \text{Eq. 5}$$

where: M is the regional tracer concentration in the myocardial wall; L is the (homogeneous) LV blood-pool concentration; R is the (homogeneous) RV blood-pool concentration; E is the regional concentration outside the heart; r_X is the regional recovery coefficient for X, where X = L, M; s_{XY} is the coefficient of spillover from Y into X, where (X, Y) = (L, M), (M, L); and X′ is the PET measurement of X; X = M, L, R.

The recovery and spillover coefficients are not independent:

$$r_M = 1 - s_{LM} - s_{RM} - s_{EM} \qquad \text{Eq. 6}$$

$$r_L = 1 - s_{ML}. \qquad \text{Eq. 7}$$

It is assumed that the concentrations M and E, the recovery and the spillover coefficients, are constant in small neighborhoods. We introduce the following assumptions and definitions:

1. The tracer uptake outside the heart (i.e., in the lungs) is low compared to that in the heart and the blood pools. Consequently, setting E to zero introduces only small errors.
2. The tracer concentration in the blood pool is homogeneous, and can therefore be represented by a single value per time frame.
3. A small region in the center of the blood pool is used to determine the values of the input function. Consequently, the recovery coefficient in that region is close to unity, and the spillover from the LV wall is small. Therefore, substitution of the value L'_0 of that region instead of L in Equation 3 is an acceptable approximation. See Figure 6 for a comparison between L and L'_0 (shrinking factor 0.4).
4. Similarly, it is assumed that R can be replaced by R′ in Equation 3 with acceptable accuracy.
5. The value of $s_{MR}s_{LM}$ is negligible.
6. The correction for the RV blood pool will be included in the compartmental model analysis. It is difficult to apply an accurate correction based on image processing methods because we do not have a reliable delineation of the RV blood pool. Therefore, we define M_r as the tracer uptake in the myocardial wall, corrected for spillover from the LV blood pool but still affected by spillover from the RV blood pool.

We then obtain the following:

$$M_r = M + s'_{MR} R' = (M' - s_{ML} L'_0)/r_M \qquad \text{Eq. 8}$$

$$s'_{MR} = s_{MR}/r_M \; L = (L' - s_{LM} M_r)/r_L. \qquad \text{Eq. 9}$$

The algorithm consists in first calculating s_{ML}, r_M, s_{LM} and r_L using image processing methods, and then applying Equations 8

and 9. The accuracy can be improved in a second iteration, using the result of Equation 9 in the re-evaluation of Equation 8. No iterations were applied here.

APPENDIX 2

The two-compartment model describes the regional tracer kinetics using a compartment with freely diffusible $^{13}NH_3$ and with (irreversibly) metabolically trapped $^{13}NH_3$ (*16*). The differential equations are:

$$\dot{Q}_1(t) = -\frac{RMBF + K_1}{V} Q_1(t) + RMBF\ C_a(t) \quad \text{Eq. 10}$$

$$\dot{Q}_2(t) = \frac{K_1}{V} Q_1(t) \quad \text{Eq. 11}$$

$$K_1 = \frac{RMBF}{0.607} \exp\left(\frac{1.25}{RMBF}\right) - RMBF \quad \text{Eq. 12}$$

$$C_T(t) = Q_1(t) + Q_2(t) \quad \text{Eq. 13}$$

$$C_m(t) = C_T(t) + LS\ C_a(t) + RSC_r(t). \quad \text{Eq. 14}$$

where: Q_1, Q_2 are the ^{13}N concentrations in the first and the second compartments (MBq/ml); RMBF is the regional myocardial blood flow (ml/min/g); K_1 is the rate constant from first to second compartment (ml/min/g); V is the distribution volume of blood in the free space (ml/g), fixed at 0.8; LS, RS are the spillover coefficients from the LV and RV blood pools into the myocardial wall; C_T is the regional ^{13}N concentration in the wall; C_m is the regional ^{13}N concentration as measured by the tomograph; and C_a, C_r are the ^{13}N concentrations in the LV and RV blood pools (MBq/ml).

After application of the CC method, the wall is corrected for both spillover and recovery. As a result, the estimate of LS should be smaller and should represent the fractional blood volume only.

The three-compartment model (*10*) assigns compartments to the vascular space (a), to the extravascular space (E) and to the metabolically trapped $^{13}NH_3$ (G). The equations are:

$$\dot{C}_E(t) = K_1C_a(t) - k_2C_E(t) - k_3C_E(t) \quad \text{Eq. 15}$$

$$\dot{C}_G(t) = k_3C_E(t) \quad \text{Eq. 16}$$

$$C_T(t) = C_E(t) + C_G(t) \quad \text{Eq. 17}$$

$$C_m(t) = (1 - LS)C_T(t) + LS\ C_a(t) + RS\ C_r(t). \quad \text{Eq. 18}$$

C_a, C_E and C_G are the ^{13}N concentrations in the respective compartments [MBq/ml].

K_1 is the $^{13}NH_3$ uptake in the extravascular space. Assuming a single-pass extraction fraction close to unity, K_1 can be regarded as the regional blood flow (ml/min/g); k_2 is the $^{13}NH_3$ washout rate (1/min); and k_3 is the metabolic trapping rate (1/min).

We have found that imposing an upper limit of 0.8 K_1 to the value of k_2 considerably reduces the noise sensitivity.

Since the LV wall was corrected for spillover and recovery, LS represents the fractional blood volume only.

For the KC method, the Equations 14 or 18 were modified to:

$$C_m(t) = (1 - LS)C_T(t) + LS\ C_a(t). \quad \text{Eq. 19}$$

The contribution from the RV is assumed to be negligible because endocardial regions were used. LS now represents the combination of fractional blood volume in the wall and spillover from the blood pool due to the limited resolution.

ACKNOWLEDGMENTS

We thank T. Stassen, L. Verhaegen and S. Vleugels for their contribution to the animal preparation and acquisition, and D. Crombez and M. Heroes for the tracer preparation. We also thank M.-C. Herregods and B. Bijnens, who supplied the echo images and the software to estimate the typical wall thicknesses. We are grateful to G. Hutchins and A. Bol for valuable advice. Lastly, we thank P. Dupont for his critical review of the paper and M. Dahlbom for organizing the digital data transfer between UCLA and K.U. Leuven. This work is supported by grant 3-0080-90 from the National Fund for Scientific Research, Belgium and by the Belgische Cardiologische Liga, Belgium.

REFERENCES

1. Hoffman EJ, Huang S-C, Phelps ME. Quantitation in positron emission computed tomography: 1. Effect of object size. *J Comput Assist Tomogr* 1979;3:299–308.
2. Ter-Pogossian MM, Bergmann SR, Sobel BE. Influence of cardiac and respiratory motion on tomographic reconstructions of the heart: implications for quantitative nuclear cardiology. *J Comput Assist Tomogr* 1982;6:1148–1155.
3. Henze EH, Huang S-C, Ratib O, Hoffman E, Phelps ME, Schelbert HR. Measurements of regional tissue and blood pool radiotracer concentrations from serial tomographic images of the heart. *J Nucl Med* 1983;24:987–996.
4. Herrero P, Markham J, Myears DW, Weinheimer CJ, Bergmann SR. Measurement of myocardial blood flow with positron emission tomography: correction for count spillover and partial volume effects. *Math Comput Model* 1988;11:807–812.
5. Ratib O, Bidaut L, Nienaber C, Krivokapich J, Schelbert HR, Phelps ME. Semiautomatic software for quantitative analysis of cardiac positron tomography studies. *SPIE, Medical Imaging II* 1988;914:412–419.
6. Kuhle WG, Porenta G, Huang S-C, Phelps ME, Schelbert HR. Issues in the quantification of reoriented cardiac PET images. *J Nucl Med* 1992;33:1235–1242.
7. Hutchins GD, Caraher JM, Raylman RR. A region of interest strategy for minimizing resolution distortions in quantitative myocardial PET studies. *J Nucl Med* 1992;33: 1243–1250.
8. Iida H, Kanno I, Takahashi A, et al. Measurement of absolute myocardial blood flow with $H_2^{15}O$ and dynamic positron emission tomography. *Circulation* 1988;78:104–115.
9. Bergmann S, Herrero P, Markham J, Wenheimer C, Walsh M. Noninvasive quantitation of myocardial blood flow in human subjects with oxygen-15-labeled water and positron emission tomography. *J Am Coll Cardiol* 1989;14:639–652.
10. Hutchins GD, Schwaiger M, Rosenspire KC, Krivokapich J, Schelbert H, Kuhl DE. Noninvasive quantification of regional myocardial blood flow in the human heart using N-13 ammonia and dynamic positron emission tomographic imaging. *J Am Coll Cardiol* 1990;15:1032–1042.
11. Muzik O, Beanlands RSB, Hutchins GD, Mangner TJ, Nguyen N, Schwaiger M. Validation of nitrogen-13-ammonia tracer kinetic model for quantification of myocardial blood flow using PET. *J Nucl Med* 1993;34:83–91.
12. Wisenberg G, Schelbert HR, Hoffman EJ, et al. In vivo quantitation of region myocardial blood flow by positron emission computed tomography. *Circulation* 1981;63:1248–1258.
13. Porenta G, Kuhle W, Sinha S, et al. Gated PET-FDG imaging permits parameter estimation of cardiac geometry: validation using gated MR imaging and echocardiography [Abstract]. *J Nucl Med* 1991;32(suppl):927.
14. Spinks TJ, Aroujo LI, Rhodes CG, Hutton BF. Physical aspects of cardiac scanning with a block detector positron tomograph. *J Comput Assist Tomogr* 1991;15:893–904.
15. Bol A, Melin JA, Vanoverschelde J-L, et al. Direct comparison of ^{13}N-ammonia and ^{15}O-water estimates of perfusion with quantification of regional myocardial blood flow by microspheres. *Circulation* 1993;87:512–525.
16. Kuhle WG, Porenta G, Huang S-C, et al. Quantification of regional myocardial blood flow using ^{13}N-ammonia and reoriented dynamic positron emission tomographic imaging. *Circulation* 1992;86:1004–1017.
17. Liow JS, Strother SC. The convergence of object dependent resolution in maximum likelihood based tomographic image reconstruction. *Phys Med Biol* 1993;38:55–70.
18. Spinks TJ, Jones T, Gilardi MC, Heather JD. Physical performance of the latest generation of commercial positron scanners. *IEEE Trans Nucl Sci* 1988;35:721–725.
19. Nuyts J, Mortelmans L, Suetens P, Oosterlinck A, De Roo M. Model-based quantification of myocardial perfusion images from SPECT. *J Nucl Med* 1989;30: 1992–2001.
20. Nuyts J, Suetens P, Oosterlinck A, De Roo M, Mortelmans L. Delineation of ECT images using global constraints and dynamic programming. *IEEE Trans Med Imag* 1991;10:489–498.
21. Silverman ME, Schlant RC. Anatomy of the normal heart and blood vessels. In: JW Hurst, RB Logue, RC Schlant, NK Wenger, eds. *The heart,* 4th ed. New York: McGraw-Hill, Inc; 1978:24.
22. Helak JW, Reichek N. Quantitation of human left ventricular mass and volume by two-dimensional echocardiography: in vitro anatomic validation. *Circulation* 1981;63: 1398–1407.
23. Bormans G, Maes A, Langendries W, et al. Metabolism of N-13-ammonia in different conditions in dogs, human volunteers and transplant patients. *Eur J Nucl Med* 1995;22:116–121.
24. Nuyts J, Dupont P, Van den Maegdenbergh V, Vleugels S, Suetens P, Mortelmans L. A study of the liver-heart artifact in emission tomography. *J Nucl Med* 1995;36:133–139.